Understanding the Hydrologic Behavior of a Small Semi-Arid Mountainous Watershed

Rajiv Prasad [1]
David G. Tarboton [1]
Gerald N. Flerchinger [2]
Keith R. Cooley [2]
Charles H. Luce [3]

Submitted to Hydrological Processes, February 2000.

Abstract

The purpose of this study is to understand hydrologic behavior at a small semi-arid mountainous watershed in order to construct a hydrologic model, which can later be scaled up to larger watersheds in the same region. We took a data intensive approach to understand the hydrologic processes acting in the watershed. Measurements used included maps of snow water equivalence surveyed manually on a 30 m grid, streamflow, precipitation, weather and radiation. Wind driven snow drifting combined with variable radiation exposure on rough terrain produces a consistent (from year to year) spatial distribution of snowpack in the watershed. Spatial variability of surface water input is identified as the dominant hydrologic process in this watershed. We use the drift factor approach to parameterize wind blown snow drifting in the watershed. The drift factors are obtained by calibration using manually surveyed snow water equivalence maps during the accumulation and drift period. Earlier studies have examined annual water balance at this watershed by dividing the watershed into three zones based on drift patterns, soil

[1] Civil and Environmental Engineering, Utah State University, Logan, UT 84322
[2] USDA Agricultural Research Service, Northwest Watershed Research Center, Boise, ID 83712

types and vegetation. We show that these zones can be obtained from the distribution of calibrated drift factors. The timing of surface water input on the zone corresponding to deep drifts on the north-facing, leeward slope corresponds closely with the timing of streamflow at the outlet. A lumped hydrologic model is developed which consists of (a) simple parameterization of evapotranspiration, (b) infiltration into the soil zone and recharge to the saturated zone, and (c) subsurface storage-discharge function. This model, applied to each of the three surface water input zones individually is shown to be sufficient to parameterize the volume and timing of runoff from this watershed.

1 Introduction

Surface water input (SWI) into a watershed consists of rainfall and/or snowmelt. The importance of correctly estimating the spatio-temporal distribution of SWI is especially important in semi-arid mountainous watersheds where most of the precipitation falls as snow and its accumulation and melt is determined by terrain properties and other weather variables. Snowpack formed during the accumulation period acts as surface water storage, delaying the infiltration of precipitation into the subsurface. Wind driven drifting in mountainous watersheds erodes snow from windward slopes and deposits it on the leeward slopes, creating a consistent spatial distribution of snowpack every year. The resulting SWI is influenced primarily by the location of the deep drifts on the leeward slopes. Windward slopes accumulate relatively thin snowpacks, which tend to melt early in the melt season, in contrast to deep drifts on leeward slopes, which melt late in the season. Previous works in this watershed (Jackson, 1994; Tarboton et al., 1995b; Jackson et al., 1996) have developed spatially distributed models which work on a regular grid. In these models, each grid cell was modeled as a snow-soil system. Snowmelt was infiltrated into the soil, which modified the water held by the soil column at each grid cell. Lateral flow in the soil was modeled explicitly using grid cell to grid cell connectivity, driven by a topographic gradient (similar to Wigmosta et al., 1994). These models were shown to model the watershed behavior reasonably well. However, these models had large data requirements and proved impractical in modeling larger scale watersheds without moving to coarser grid sizes. In this paper we use the knowledge gained from earlier studies and results obtained from extensive data analysis to identify important hydrologic processes and develop a methodology to build simpler hydrologic models, which describe the hydrologic behavior at the watershed scale. A

simple hydrologic model which is driven by SWI computed from the spatially distributed snowpack is shown to be sufficient to parameterize the volume and timing of runoff from a first order watershed. This approach will be used in forthcoming papers to upscale our modeling to larger watersheds.

2 Study site and available data

Reynolds Creek Experimental Watershed (RCEW) is a 233.5 km^2 semi-arid mountainous watershed located in southwestern Idaho (Fig. 1) and has been the focus of intensive hydrometeorologic and geologic instrumentation and investigation over the last three decades (Hamon, 1973; Stephenson and Freeze, 1974; Winkelmaier, 1987; Hanson, 1989; Duffy et al., 1991; Stevens, 1991; Flerchinger et al., 1992 among others). The watershed is maintained by the Northwest Watershed Research Center (NWRC), Boise, ID, a part of the Agricultural Research Service, U. S. Department of Agriculture. Elevations in the watershed range from 1097 to 2237 m. Mean annual precipitation varies with elevation and ranges from 229 to 1107 mm. The watershed is almost entirely sagebrush rangeland. Approximately 9% of the area is cultivated/burned/seeded and about 5% is forested with scattered Douglas fir, aspen and alpine fir. The main waterway of Reynolds Creek has a length of 25.1 km and overall slope of 4%. The hydrology of the watershed is mainly snowmelt driven. Channel flow is sustained by groundwater recharged by infiltration of snowmelt.

Upper Sheep Creek (USC) is a 0.25 km^2 first order watershed within Reynolds Creek Experimental Watershed (Fig. 1). This watershed has been the location of intensive study of the distribution of snow over the period 1982 to 1996. A 30 m grid over the watershed defines 255

locations where snowpack has been measured at approximately 2 week intervals during the winter (as described by Cooley, 1988). In particular, nine snow surveys were conducted during water year 1992-93, thereby establishing the spatio-temporal distribution of snow accumulation and melt at USC. Snow water equivalence maps derived from the snow surveys are shown in Fig. 2. This study focused on the water year 1992-93. The hydrometeorologic instrumentation network at USC is described in detail by Flerchinger et al. (1998).

The topography depicted in figures 1 and 2 is from a 30 m digital elevation model (DEM) of the watershed. This was obtained from averaging a commercial high resolution 10 m DEM developed from USGS 1:24000 maps for Reynolds Creek Experimental Watershed.

3 Modeling surface water input

The field snow surveys provide snapshots in time of the spatial pattern of snow accumulation and ablation (Fig. 2). In order to relate observed changes in snowpack to surface water input, which drives the hydrologic response, we need to estimate and interpolate melt rates between these measurements. Here a snowmelt model is used for this interpolation. Apart from some specialized wind blowing models (e.g. Pomeroy and Gray, 1995; Liston and Sturm, 1998) most physically based snowmelt models do not include a description of wind-driven drift; indeed, they are point models, and application of these models to a regular grid needs to account for lateral snow exchanges.

Our approach here is to apply a point snowmelt model to represent snowmelt, and absorb the effects of wind-driven drift into a drift factor (Jackson, 1994). The drift factor at a point is a factor by which gage snowfall must be multiplied to equate measured and modeled snow water

equivalence (SWE) on the ground. It is used to describe the propensity of a location to accumulate extra snow through drifting (drift factor > 1), or to lose snow due to scouring (drift factor < 1). These drift factors vary spatially over the domain and are multiplied with observed snowfall to model snowfall redistribution by wind. This approach approximates drifting which follows snowfall as occurring concurrently with snowfall. This approach also amounts to an assumption of linearity in the spatial pattern of snow accumulation. If precipitation is doubled, the spatial pattern is assumed to remain the same with double the amount at each location. In order to estimate the drift factors over the watershed, a physically-based point snowmelt model called the Utah Energy Balance (UEB) snow accumulation and melt model (Tarboton et al., 1995a; Tarboton and Luce, 1996) is applied to each grid cell at USC. Using the model in this way provides an approach to account for the melt that occurs during accumulation and drifting. Snowmelt during the accumulation and drift period is usually small, yet significant. The first three manually surveyed snow water equivalence maps during 1992-93 (dates 02/10/1993, 03/03/1993 and 03/23/1993) are used to carry out a point-by-point calibration. We used an objective function which was the sum of the signed differences between modeled and measured snow water equivalence on these three dates. The objective function was monotonic with respect to the drift factor. Drift factor at each grid cell is thus obtained as the value which makes the objective function zero at that grid cell. The snowmelt model was run at an hourly time step driven by observations of radiation, precipitation, air temperature, humidity, and wind speed. Other parameters of the UEB model were fixed at their recommended values (Tarboton and Luce, 1996). Fig. 3 shows the map of calibrated drift factors. These drift factors differ from those previously reported (Jackson, 1994; Tarboton et al., 1995b) because they are on a north-

aligned grid and calibrated to the 1992-93 observations. The previously reported drift factors were calibrated against 1985-86 data on a skewed grid and used in a split sample test to compare against data from 1992-93. The 1992-93 drift factors are slightly smaller than the 1985-86 drift factors consistent with the observation of less wind redistribution of snow in 1992-93. Drift factors calibrated to the year of interest are used here because our intent is to obtain the best estimates of surface water input based on all information available for this year so we can understand and model the hydrologic response.

The physically based point snowmelt model, UEB (Tarboton and Luce, 1996) could also have been used to estimate surface water inputs. However, even with calibrated drift factors we found that our current physically based model still differs noticeably from the measurements in its reproduction of measured snow water equivalence (see Figs. 4 and 5). Fig. 4 shows the time series of observed and modeled basinwide average SWE. Fig. 5 shows the comparison between observation-based and modeled watershed snow loss rates over the inter-measurement periods. Observation-based cumulative surface water input is calculated as the difference between basinwide cumulative precipitation estimated from measurements and drift factors and measured snow water equivalence on any date. The observation-based average snow loss rates for inter-measurement periods were then calculated from the cumulative values. Fig. 5 shows that UEB underestimates the snow loss rate during the first inter-measurement period (Feb. 10 – Mar. 3, 1993). Snow loss rates computed during the next two inter-measurement periods (Mar. 3 – Mar. 23, 1993, and Mar. 23 – Apr. 8, 1993) are overestimated by UEB. Approximately two-thirds of the snow modeled by UEB at the start of these two inter-measurement periods (approximately 0.3 m on March 3, 1993, as shown by the dotted line in Fig. 4) melts during this time (UEB

modeled basin average SWE on April 8 is about 0.1 m, as shown by the dotted line in Fig 4). UEB underestimated the snow loss rate during the inter-measurement periods Apr. 8 – Apr. 15, 1993, overestimated it slightly during Apr. 15 – Apr. 29, 1993, was very close during Apr. 29 – May 12, 1993, and underestimated the snow loss rates during the last two inter-measurement periods, May 12 – May 19, 1993, and May 19 – May 25, 1993. The underestimation of snow loss rate during the last two inter-measurement periods is partly due to the fact that as per UEB, almost all snow had melted by that time. As shown in Fig. 5, the snow loss rate predicted by an index-based snowmelt model is closer to the observation-based average snow loss rates for all inter-measurement time periods except the three during Apr. 8 – May. 12. The index-based snowmelt model is described below. It can be seen that the index-based model tracks the basin average snow water equivalence more accurately than UEB (see Fig. 4).

Since the focus of this study was to understand the hydrologic response due to surface water input patterns, we wanted to ensure that surface water inputs corresponded as closely with measurement as possible. Therefore we chose to sidestep the discrepancies with the physically based model and develop an index-based approach to estimate snowmelt and surface water inputs. We are thus replacing the physical rigor, transportability and generality of the UEB model, with simplicity and accuracy for this specified setting. The index-based snowmelt model still uses the drift factors calibrated using UEB. Early in the season, drifting and accumulation dominate, and melting is a secondary effect, therefore the drift factors estimated with UEB are still felt to be our best estimate of actual drift effects.

The index-based approach uses air temperature and net radiation to estimate snow melt at each grid cell.

$$M = M_f \cdot \max[R \cdot (T_a - T_b), 0] \quad (1)$$

Here M is rate of snowmelt in m/hr, M_f is a parameter (the melt factor, m/hr/(W/m^2)/^{o}C), T_a is air temperature (^{o}C), T_b is a reference base temperature (0 ^{o}C) and R is net radiation. This multiplicative form of the index model was the best of several we tried and has also been used by others previously (Riley et al., 1966; Sharma and Tarboton, 1995). Air temperature at each grid cell is adjusted from measurement at a reference location using an average lapse rate.

Measured incoming solar radiation is split into direct and diffuse components (for details, see Appendix). Incident radiation at a grid cell is composed of incoming direct shortwave, incoming diffuse sky and incoming longwave radiation. Direct radiation is adjusted for terrain slope, aspect and shading. Diffuse and longwave radiation components are adjusted for sky view fraction at each grid cell. Specifically we estimate net radiation using

$$R = (1 - A) \cdot (R_{dir} + R_{dif}) + R_{lw,net} \quad (2)$$

where A is snow surface albedo taken as 0.85. R_{dir} and R_{dif} (W/m^2) are the terrain adjusted direct and diffuse components of incident solar radiation, and $R_{lw,net}$ is the net longwave radiation (see Appendix for details).

Air temperature is used to partition precipitation into snow and rain (U.S. Army Corps of Engineers, 1956). The fraction of precipitation falling as snow is given by:

$$
\begin{aligned}
f_{snow} &= 1.0 && when\ T_a < T_s \\
&= \frac{T_r - T_a}{T_r - T_s} && when\ T_s \le T_a \le T_r \\
&= 0.0 && when\ T_a > T_r
\end{aligned}
\tag{3}
$$

where T_r (= 1 ^{o}C) is the air temperature above which all precipitation is assumed to fall as rain, and T_s (= -3 ^{o}C) is the air temperature below which all precipitation is assumed to fall as snow. Rain is assumed to pass through any snow already present on ground and immediately add to surface water input. Snowfall is adjusted for wind induced drifting, using the drift factor f_{drift} for each grid cell, and is given as:

$$P_{snow} = f_{snow} \cdot f_{drift} \cdot P \tag{4}$$

where P is the measured precipitation (m).

SWE at any grid cell at the end of next time step is determined from the mass balance equation:

$$SWE_t = SWE_{t-1} + (P_{snow,t} - M_t) \cdot \Delta t \tag{5}$$

This snowmelt model (Pseudo-Distributed Index-based Model for Snowmelt, PDIMS) was calibrated at USC to obtain the melt factor. The spatial distribution of snowmelt is influenced largely by spatial variation in radiation and air temperature, which have strong diurnal cycles and vary on a short time scale. Radiation and air temperature are also strongly influenced by terrain

properties such as slope, aspect, sky view factor and terrain shading. We assume that the incorporation of topographic effects into R and T_a accounts for these effects. Therefore melt factors are assumed to be uniform in space and to vary on a much longer time scale. Here we assume melt factors to be constant on a monthly time scale. This gives us 5 melt factors, one each for January through May. We found that the model is insensitive to the values of melt factor during other months when there is minimal snowmelt (June through December). The objective function used during calibration is the sum of square of differences between the modeled and measured SWE at each grid cell in the watershed for each of the nine SWE measurements:

$$F\left(\{M_f\}\right) = \sum_{\vec{x}\in\vec{X}} \sum_{t=1}^{9} \left\{SWE_{\mathrm{mod}}(\vec{x},t) - SWE_{obs}(\vec{x},t)\right\}^2 \qquad (6)$$

where $\{M_f\}$ is the set of melt factors being calibrated, $\vec{x}$ refers to the location of a specific grid cell, $\vec{X}$ is the set of all grid cells that constitute the watershed, and t is the index identifying a SWE map measured by the snow surveys at USC. Parameters of PDIMS were calibrated for three configurations:

(a) melt factor varying for each month during January through May (5 Par PDIMS),

(b) one melt factor during January and February which are primarily accumulation months, and another during March through May which are primarily melt months (2 Par PDIMS), and

(c) temporally constant melt factor (1 Par PDIMS).

Calibration was carried out using an interactive program called NLFIT (Kuczera, 1994). PDIMS was run on an hourly time step. Modeled SWE maps at 1300 hours on the dates when SWE measurements were carried out were used to compute the objective function. It was found that the 2 Par PDIMS and 1 Par PDIMS give noticeably poor time history of basin average SWE as compared to 5 Par PDIMS. Since we need an accurate surface water input time series to assess the hydrologic behavior of the watershed, we chose to use 5 Par PDIMS as the snowmelt model. Table 1 shows the calibrated melt factors for 5 Par PDIMS configuration. Fig. 4 includes the time history of observed and modeled basinwide average SWE from PDIMS. This follows the observations more closely than the UEB simulation. Fig. 5 includes snow loss rates from the PDIMS model. Again these compare more closely to the observation based loss rate estimates. Fig. 6 shows the modeled (5 Par PDIMS) SWE maps. Fig 7 shows the pointwise comparison between the observed and modeled SWE. R^2 is computed for the modeled SWE maps as:

$$R^2 = 1 - \frac{\sum_{\vec{x} \in \vec{X}} \left[SWE_{\mathrm{mod}}(\vec{x}) - SWE_{obs}(\vec{x}) \right]^2}{\sum_{\vec{x} \in \vec{X}} \left[SWE_{obs}(\vec{x}) - \overline{SWE}_{obs} \right]^2} \qquad (7)$$

where $\overline{SWE}_{obs}$ is the mean of the observed SWE map.

Comparing the index based PDIMS and UEB simulations in figures 4 and 5 shows the advantage of using the index-based model for estimates of surface water inputs at Upper Sheep Creek.

5 Analysis of surface water input at Upper Sheep Creek

Surface water input is defined as the sum of rainfall and snowmelt at a given time step at any grid cell. SWI at USC for 1992-93 water year was computed using the 5 Par PDIMS. Research in the past has indicated three snowmelt zones at USC (Cooley, 1988). Snow on the windward southwest facing slope melts early in the season. Snow on the northeast facing slope melts in two stages – a general melt period when most of the relatively thin snowpack on the northeast facing slope is consumed, and a drift melt period when the deep drift which forms on the leeward northeast facing slope melts. In order to identify these three SWI zones at USC, we examined the distribution of the drift factors at USC, which, because all snow eventually melts, is equivalent to the distribution of cumulative SWI throughout the season (Fig. 8). It can be seen that there are roughly three modes on this histogram that can be used to cluster or group the grid cells of USC into SWI zones. The first cluster extends from drift factor values of 0.0 to about 0.5, the second cluster extends from 0.5 to 1.0 and the third for all drift factors greater than 1.0. This gives us a basis for subdividing USC into three zones based on cumulative SWI (or, equivalently, drift factors). These three zones are: zone 1: early snowmelt on southeast facing slope corresponding to drift factors between 0.0 and 0.5; zone 2: general snowmelt on northeast facing slope corresponding to drift factors between 0.5 and 1.0, and zone 3: drift snowmelt on northeast facing slope corresponding to drift factors greater than 1.0. Subdividing USC using the criterion outlined above leads to the three zones shown in Fig. 8. These zones do correspond approximately to the three snowmelt zones described by Cooley (1988) and Flerchinger et al. (1998). The importance of this subdivision becomes apparent when we examine the time series

of cumulative SWI into each of these zones (Fig. 9). The solid line in Fig. 9 is the basinwide SWI (area weighted average of SWI for the three zones). Measured runoff at USC during 1992-93 is shown in Fig. 10. Outflow starts around the beginning of May. The whole watershed becomes snow free at the beginning of June. It can be seen on Fig. 9 that zones 1 and 2 do not get any appreciable SWI during May, in contrast to zone 3, which shows a rapid rise in SWI during this time period, and corresponds closely with the rise in the outflow hydrograph. The rise in cumulative graphs of SWI beyond June is all due to rainfall.

Furthermore, the potential evapotranspiration for this period, evaluated using the model described below, was 967.8 mm, 862.3 mm and 724.0 mm for zones 1 to 3 respectively. This is greater than the surface water input in zones 1 (460.0 mm) and 2 (665.3 mm), but less than the surface water input in zone 3 (1263.2 mm), indicating that zone 3 must generate runoff, whearas in zones 1 and 2 there is potential for all surface water input to be lost to evapotranspiration.

This behavior leads us to believe that almost all of watershed outflow is generated by the SWI that occurs on zone 3 during May generated by the melting of the deep snowdrift on this zone. These insights suggest that a lumped hydrologic model based on these three SWI zones should perform well in terms of predicting watershed outflow at USC.

6 Dominant Zone Hydrologic Model (DZHM)

Based on insights gained from the distribution of SWI at USC, we developed a hydrologic model, which works on what we call dominant zones of the watershed. The overall behavior of the watershed is determined by the aggregation of individual zone behavior. In our case, these dominant zones are identified as the three SWI zones described above. In general, these zones

should be determined from important hydrologic behavior in the watershed of interest. The components of DZHM are described here.

Surface Water Input: Surface water input into the soil is computed using PDIMS, as described in earlier sections.

Evapotranspiration: Potential evapotranspiration is computed from Priestly-Taylor equation. Actual evapotranspiration is then computed depending on moisture availability in the soil store.

$$PET = a \frac{\Delta}{\Delta + g} \frac{R_a}{l \cdot r_w} \tag{8}$$

$$AET = K_{veg} \cdot f_{AET} \cdot PET \tag{9}$$

where a is the Priestly-Taylor coefficient (1.74 for arid climate, Shuttleworth, 1992 p4.17), Δ is the gradient of the saturated vapor pressure – temperature curve at air temperature, g is the psychometric constant at air temperature and pressure, l is the latent heat of vaporization of water (kJ/kg), r_w is the density of water (kg/m^3), R_a is a measure of available energy (net short- and long-wave radiation, kJ/m^2/hr), f_{AET} is the soil moisture dependent ratio of actual to potential evapotranspiration parameterized as shown in Fig. 11 similar to Shuttleworth (1992 Fig 4.4.3, p4.46), and the coefficient K_{veg} accounts for vegetation type. The parameters involved in the

evapotranspiration component are K_{veg}, and moisture contents at saturation q_s, field capacity q_r and permanent wilting point q_w.

Soil Zone: The soil zone acts as a temporary store for infiltrated water. Evapotranspiration extracts moisture from this store. The soil zone drains to the saturated zone. Hydraulic conductivity in the soil zone is assumed to decrease exponentially with depth. The active capacity of the soil zone is divided into components between the volumetric moisture content at saturation q_s, field capacity q_r and permanent wilting point q_w. We define $Dq_1 = q_s - q_r$, $Dq_2 = q_r - q_w$ and $Dq = Dq_1 + Dq_2$. The soil zone is characterized by a depth z_r (m), which gives a capacity parameter:

$$SOILC = z_r \cdot (q_s - q_w) = z_r \cdot (\Delta q_1 + \Delta q_2) = z_r \cdot \Delta q \qquad (10)$$

The state of the soil zone is denoted by *SR* (m), which represents the depth of water stored in the soil zone. Potential rate of infiltration is computed using a Green-Ampt like formulation:

$$i = K_o \cdot e^{-f \cdot z_f} \frac{z_f + y_f}{z_f} \qquad (11)$$

with

$$z_f = \frac{SR}{\Delta q} \tag{12}$$

where K_o is the hydraulic conductivity of soil at the surface (m/hr), f is the parameter that defines the rate of exponential decrease of hydraulic conductivity with depth (1/m) and y_f is the wetting front soil suction head (m). This assumes that for the purposes of infiltration excess calculation all moisture in the soil zone is in a saturated wedge at the surface above a wetting front.

Drainage from the soil zone to the saturated zone is computed using:

$$r_d = K_o \cdot e^{-f \cdot z_r} \left(\frac{\max(0, SR - z_r \cdot \Delta q_2)}{z_r \cdot \Delta q_1} \right)^c \tag{13}$$

This assumes that for the purposes of drainage calculations that the moisture content is uniform over the soil zone. Drainage only occurs when moisture content is in excess of field capacity. The maximum drainage rate is assumed to be hydraulic conductivity at the base of the soil zone with drainage reducing as moisture content reduces according to a pore disconnectedness parameter c. These are recognized to be gross simplifications. Nevertheless they capture the major sensitivities in a relatively simple way. The parameters involved in the soil zone component are K_o, f, z_r, y_f, c, and moisture contents at saturation q_s, field capacity q_r and permanent wilting point q_w.

Saturated Zone (baseflow): Our analysis of saturated zone storage and measured discharge showed evidence that the saturated zone at USC acts as a bucket-like store, which overflows when storage exceeds a threshold. The relationship between storage and discharge beyond the threshold was not clearly established from analysis of data, and we chose to employ a general power-function like relationship, given by:

$$\begin{aligned} Q_b &= 0 && if \quad \bar{z} > z_i \\ &= K_o \cdot e^{-f \cdot \bar{z}} \cdot \left(\frac{z_i - \bar{z}}{z_i} \right)^h && if \quad \bar{z} \le z_i \end{aligned} \tag{14}$$

where Q_b is baseflow (m/hr), z_i is the threshold (m), h is the parameter of the saturated zone power-function storage-discharge relationship. The state of the subsurface storage is denoted by $\bar{z}$ (m), which is the average depth to the water table measured from the soil surface. Parameters involved in saturated zone flow are z_i, h, K_o and f.

Streamflow: In this model, we do not use an explicit streamflow routing scheme. Rainfall excess surface runoff can be generated at the soil zone surface if SWI during a time step exceeds the net water holding capacity of the soil zone or potential infiltration rate. In USC essentially no overland flow is observed and in the model runs surface runoff is rarely generated. Therefore we decided that effort to model routing of overland flow was not warranted and held this excess water in a surface store for reinfiltratation during subsequent time steps. The streamflow at the outlet of the watershed is taken as the sum of the baseflows generated from the three zones. The

time delay between the baseflow response and its appearance at the basin outlet is assumed to be zero.

7 Calibration of DZHM

DZHM is used to implement a 3-zone model for USC. The parameters q_s, q_r, q_w, z_r and c were not calibrated. They were set at values given in Table 2. The soil moisture content parameters were estimated for each zone based on soil texture information, and some measured soil moisture data at the start of the 1992-93 water year, when the moisture conditions were very dry. We did not have any information to determine the drainage properties of the soils at USC, and so we decided to set c to 1.0, which results in linear scaling of the drainage rate by the ratio of available moisture ($SR - z_r \cdot \Delta q_2$) to drainable capacity ($z_r \cdot \Delta q_1$). NLFIT was used to calibrate the remaining parameters. Of these remaining parameters, all were assumed to be identical across the three zones, except for K_{veg}, which was used to characterize the vegetation differences between zones. The calibration was carried out in two phases. In the first phase, the parameter K_{veg} was calibrated for each zone, while keeping the values of K_o and f fixed at some nominal values. This calibration used measured ET data at USC (Flerchinger et al., 1998). Fig. 12 shows modeled and measured cumulative ET after this calibration for each zone.

In the second phase of calibration, the saturated zone parameters z_i and h were calibrated along with K_o and f. These parameters were assumed to be uniform across the three zones. This phase of calibration used measured 1992-93 streamflow at the outlet of USC. Computed ET after the second phase of calibration was found to be insensitive to changes in the values of K_o and f, which occurred during the transition from phase one to phase two. We decided, therefore,

not to iterate on the two phases of the calibration. The values of all parameters after calibration are shown in Table 2.

8 Mass balance components at USC during 1992-93

Basinwide mass balance components as simulated by the calibrated DZHM are shown in Table 3 and Fig. 13. There was 715.2 mm of surface water input (rainfall + snowmelt) during the simulation period (Oct. 1, 1992 – Aug. 16, 1993). The simulated ET accounted for 407.8 mm, which is reasonably close to the estimate given by Flerchinger et al. (see Table II in Flerchinger et al., 1998). Runoff accounted for 60.6 mm, which compares favorably with the measured volume of runoff (59.7 mm). The rest of the water was stored in the soil zone (20.1 mm) and the saturated zone (226.7 mm). These storage component values differ from those reported by Flerchinger et al. (20.1 mm vs. 100 mm for soil zone and 226.7 mm vs. 75 mm for the saturated zone, see Table II in Flerchinger et al., 1998). These discrepancies may be due to difficulties associated in interpreting point measurements to estimate zonal averages, differences in definition of soil and saturated zones, interpretation of model state variables compared to measurements, and due to the simple structure of the subsurface model used in DZHM. Overall, basinwide mass balance components agree well with observations. Table 3 also shows zonal mass balance components. Surface water input for zones 1 and 2 was substantially less than the potential evapotranspiration. For zone 3, however, surface water input was greater than potential evapotranspiration. On zones 1 and 2, a large fraction of surface water input was used to satisfy the evapotranspiration demand, and the rest of the water was not sufficient to raise the water table to the threshold in order to produce runoff. On zone 3, although the absolute actual

evapotranspiration was larger than those on zones 1 and 2, it was a smaller fraction of the surface water input compared to the other zones. The relatively large fraction of surface water input available for infiltration on zone 3 raised the water table to the threshold, and resulted in all runoff produced at USC. The spatial variability of surface water input, which is a result of the wind-driven snow drifting, controls the amount and timing of recharge at USC, and is thus identified as the dominant hydrologic process.

9 Summary and conclusions

In this paper, we used an extensive hydrometeorological dataset to identify hydrologic behavior at a small semi-arid mountainous watershed. The hydrologic behavior of the watershed was mainly influenced by the spatial variability of surface water input. The variability of surface water input was a direct result of the wind-driven redistribution of snow. Wind induced drifting was parameterized by the drift factor concept. Drift factors were obtained by calibration against measured snow water equivalence maps. A physically-based, energy-balance snowmelt model was used to estimate early season melt during the calibration. This drift factor map was used to parameterize the wind-induced snow drifting over the watershed in absence of explicit lateral snow exchange over the grid cells.

Surface water input was computed using a simple, index-based snowmelt model, PDIMS. The parameters of PDIMS were obtained by calibration against measured snow water equivalence maps. The calibration was carried out using an interactive optimization software, NLFIT. The space-time evolution of snowpack and surface water input during one snow accumulation, drift and melt season was excellently modeled using the UEB calibrated drift

factors and 5 Par PDIMS. The distribution of drift factors was used to delineate zones of surface water input. These zones corresponded well with snowmelt zones described by past investigations at USC. Comparison of the cumulative surface water input time series with the measured runoff from USC suggested that almost all of the measured outflow resulted from the surface water input from the deep drifts which formed on the leeward, northwest facing slope of USC. The timing of measured USC outflow also corresponded closely with the timing of SWI into the zone corresponding to leeward, northwest facing slope where the deep drifts form. Based on these insights, we developed a simple lumped hydrologic model, DZHM, which was applied to each of the three SWI zones individually. NLFIT was used to calibrate DZHM in two phases, first against ET data and then against measured streamflow. The aggregate water balance values reported in Table 3 agree favorably with those reported by Flerchinger et al. (1998), except for the aggregate storage changes in the soil zone and in the saturated zone. We suspect that these discrepancies may be partly due to difficulties inherent in interpreting point-scale measurements to estimate zonal average conditions, differences in definition of soil and saturated zones, interpretation of model state variables compared to measurements, and partly due to the simplified structure of the soil zone representation in DZHM.

We have shown in this paper that small-scale hydrology at a first-order subwatershed in Reynolds Creek Experimental Watershed is controlled by the magnitude and timing of surface water input into the soil, which depends on the spatial variability of snowpack accumulation during winter. Once we correctly identified and represented the spatial variability of surface water input, a simple lumped hydrologic model was sufficient to parameterize the hydrologic behavior at the scale of the first-order subwatershed. In order to upscale our understanding to

model the hydrologic behavior of larger watersheds within RCEW, we believe it is necessary to establish the spatial variability of snowpack accumulation and melt. At scales larger than Upper Sheep Creek, it is impractical to conduct manual snow surveys. Wind blowing snow transport models (e.g., Pomeroy and Gray, 1995; Liston and Sturm, 1998) may be a viable alternative for estimating terrain related drift factors. Work along these lines is in progress.

Appendix: The radiation model

This appendix describes the methodology adopted for computing spatially distributed net radiation. The purpose of this method is to estimate direct shortwave, diffuse shortwave sky and net longwave radiation components acounting for the effects of terrain (i.e. slope, aspect and shading) so as to obtain spatially distributed radiation inputs suitable for spatially distributed snowmelt and evapotranspiration modeling.

A1. Shortwave radiation

Observed global radiation (direct beam plus diffuse sky) measurements recorded by a horizontally mounted pyranometer are compared to extraterrestrial radiation (radiation without atmospheric effects) for each model time step to infer the absorption and scattering properties of the atmosphere. These inferred properties are then used to model radiation at each point in a spatially distributed model, accounting for the effects of terrain (slope, aspect and shading).

Extraterrestrial radiation

The instantaneous extraterrestrial radiation flux i_{et} on a horizontal surface is given by

$$i_{et} = I_0 \cdot \cos y \qquad \text{(A1)}$$

where I_0 is the solar constant (1367 W m^{-2}), and y is the solar zenith angle given by (Dingman, 1994)

$$\cos y = \sin f \cdot \sin d + \cos f \cdot \cos d \cdot \cos wt \qquad \text{(A2)}$$

where f is the latitude, w is the angular velocity of earth's rotation (0.2618 rad h^{-1}), t is the time in number of hours before (-ve) or after (+ve) true solar noon, and d is the declination of the sun given by

$$d = \frac{23.5p}{180} \cdot \sin\left[\frac{2p}{365} \cdot (D - 82)\right] \qquad \text{(A3)}$$

where D is the Julian day ($1 \le D \le 365$ or 366).

The instantaneous extraterrestrial radiation flux is integrated over a time step (t_1, t_2) to give the integrated extraterrestrial radiation flux on a horizontal plane I_{et}:

$$I_{et} = \frac{1}{(t_2 - t_1)} \cdot \int_{t_1}^{t_2} i_{et}\, dt = \frac{I_0}{(t_2 - t_1)} \cdot \int_{Max(t_1, t_{sr})}^{Min(t_2, t_{ss})} cos?\; dt \qquad \text{(A4)}$$

where t_{sr} and t_{ss} denote sunrise and sunset times and the Max and Min ensure that the period of integration does not include time when the sun is below the horizon. We use the analytical expression based on Dingman (1994 p535) to evaluate this.

Direct and diffuse components of extraterrestrial radiation

The hourly clearness index, k_t, is defined as (see page 77, Duffie and Beckman, 1991):

$$k_t = \frac{I_{swobs}}{I_{et}} \tag{A5}$$

where I_{swobs} is the measured global radiation averaged over the measurement time period. The diffuse fraction of global radiation is given by (Erbs et al., 1982):

$$\begin{aligned} f_{dif} &= 1.0 - 0.09 \cdot k_t && \text{for } k_t \le 0.22 \\ &= 0.9511 - 0.1604 \cdot k_t + 4.3380 \cdot k_t^2 - \\ &\quad 16.6380 \cdot k_t^3 + 12.336 \cdot k_t^4 && \text{for } 0.22 < k_t \le 0.80 \\ &= 0.165 && \text{for } k_t > 0.80 \end{aligned} \tag{A6}$$

and the direct and diffuse components of the measured global radiation are given as

$$\begin{aligned} I_{dif} &= f_{dif} \cdot I_{swobs} \\ I_{dir} &= (1 - f_{dif}) \cdot I_{swobs} \end{aligned} \tag{A7}$$

We note here that if the pyranometer location is significantly influenced by terrain shading (e.g., if the pyranometer is located in a valley), then the measured global radiation I_{swobs} will be reduced relative to an open horizontal location, resulting in reduction in k_t and increase in f_{dif}. This effect will be worse near sunrise and sunset. Since the radiation near sunrise and sunset is a small fraction of radiation received during the whole day, we neglect this effect.

Estimation of direct and diffuse radiation on grid cells

The extraterrestrial radiation flux on a sloping plane is computed by using the equivalent plane concept (Dingman, 1994). The difference in longitude between the location of the original slope and that of the equivalent plane is given by

$$\Delta\Omega = \tan^{-1}\left(\frac{\sin ß \cdot \sin a}{\cos ß \cdot \cos f + \sin ß \cdot \sin f \cdot \cos a}\right) \quad \text{(A8)}$$

where b is the slope of the plane (+ve downward), and a is the aspect (direction) of the slope (counterclockwise from south). The equivalent latitude for the sloping plane is given by

$$f_{eq} = \sin^{-1}(\cos ß \cdot \sin f - \sin ß \cdot \cos a \cdot \cos f) \quad \text{(A9)}$$

Now, the incidence angle of the direct solar beam on the sloping plane y_{eq} is given by

$$\cos y_{eq} = \sin f_{eq} \cdot \sin d + \cos f_{eq} \cdot \cos d \cdot \cos(wt + \Delta\Omega) \quad \text{(A10)}$$

and the integrated extraterrestrial solar radiation flux over the time interval (t_1, t_2) per unit horizontal area at a location $\vec{x}$ can be expressed as:

$$R_{et}(\vec{x}) = \frac{I_0}{(t_2 - t_1)\cdot \cos b} \cdot \int_{Max(t_1, t_{sr})}^{Min(t_2, t_{ss})} \cos ?_{eq}\ dt \qquad \text{(A11)}$$

In evaluating the integral in eqn. (A11) t_{sr} and t_{ss} are evaluated based upon horizon angles to account for terrain shading where present. As before the analytical expression for this integral based on Dingman (1994 p535) is used. The global radiation at location $\vec{x}$ now can be estimated by using the hourly clearness index as

$$R_{sw}(\vec{x}) = k_t \cdot R_{et}(\vec{x}) \qquad \text{(A12)}$$

The direct radiation at any grid cell $\vec{x}$ is

$$R_{dir}(\vec{x}) = (1 - f_{dif}) \cdot R_{sw}(\vec{x}) \qquad \text{(A13)}$$

The diffuse radiation at the grid cell $\vec{x}$ is adjusted for the sky view factor $V_d(\vec{x})$. The sky view factor is based on the assumption of isotropic sky radiation and is defined as the ratio of the radiation incident on a point accounting for slope, aspect and terrain obstructions, to the equivalent radiation incident on an unobstructed horizontal surface. The sky view factor and horizon angles are evaluated following methods given by Dozier and Frew (1990). The diffuse sky radiation flux at the grid cell $\vec{x}$ is thus given by

$$R_{dif}(\vec{x}) = f_{dif} \cdot R_{sw}(\vec{x}) \cdot V_d(\vec{x}) \qquad \text{(A14)}$$

A2. Longwave radiation

Incoming longwave radiation from the atmosphere at any location $\vec{x}$, is estimated using the air temperature T_a (K) adjusted for an average lapse rate, cloudiness factor (f_{cloud}), and the sky view factor.

$$R_{lwi}(\vec{x}) = \{ f_{cloud} \cdot e_{cloud} + (1 - f_{cloud}) \cdot e_{air} \} \cdot s \cdot T_a(\vec{x})^4 \cdot V_d(\vec{x}) \quad \text{(A15)}$$

where s is the Stefan-Boltzmann constant (5.67×10^{-8} W m^{-2} K^{-4}). Emissivity of clouds (e_{cloud}) is set to 1.0, and emissivity of air (e_{air}) is computed using Satterlund's (1979) formula based on humidity:

$$e_{air} = 1.08 \cdot \left[1 - \exp\left\{ -\left(\frac{e_a}{100} \right)^{T_a / 2016} \right\} \right] \quad \text{(A16)}$$

where e_a is the vapor pressure in Pa.

The cloudiness factor f_{cloud} is an estimate of the fraction of the sky that is cloud covered and is estimated as the ratio of the direct shortwave radiation to what would be possible under clear skies. We assume that the atmospheric transmission factor for extraterrestrial radiation does not exceed 0.8 (see for example, Shuttleworth, 1992 p4.5), the remainder of radiation being absorbed or back scattered into space. Eqn. (A9) gave the maximum fraction of direct radiation as 0.835.

Combining this with the maximum transmission factor of 0.8 for extraterrestrial radiation suggests a maximum value for the transmission factor for direct radiation:

$$t_{dir,max} = 0.8 \times 0.835 = 0.668 \quad \text{(A19)}$$

The actual atmospheric transmission factor for direct radiation is estimated as

$$t_{dir} = k_t \cdot (1 - f_{dif}) \quad \text{(A20)}$$

Therefore the cloudiness factor can be estimated as:

$$f_{cloud} = 1 - \frac{t_{dir}}{t_{dir,max}} = 1 - \frac{t_{dir}}{0.668} \quad \text{(A21)}$$

The above approach to estimate the cloudiness factor cannot be used during nighttime because I_{et} is zero and k_t is not determinable. During nighttime we use the daytime average of k_t weighted by I_{et}.

Outgoing longwave radiation from the snow cover is estimated using a snow surface temperature T_s (K) set to the minimum of 273 K and the air temperature.

$$R_{lw,snow}(\vec{x}) = e_{snow} \cdot s \cdot T_s(\vec{x})^4 \quad \text{(A22)}$$

Outgoing longwave radiation from the ground is computed based on a ground temperature assumed equal to the air temperature T_a (K).

$$R_{lw,ground}(\vec{x}) = e_{ground} \cdot s \cdot T_a(\vec{x})^4 \quad \text{(A23)}$$

The emissivity of snow was taken as 0.99 (Tarboton and Luce, 1996), and that of the ground was taken as 0.97 (see Table D-1 in Appendix D, Dingman, 1994).

Terrain emitted longwave radiation incident on a given location is computed as a composite of longwave emission from the snow covered fraction (A_f) and bare ground fraction (1-A_f) adjusted for the ground view factor (1-V_d):

$$\begin{aligned} R_{lwi,terrain}(\vec{x}) \quad = \quad & \{A_f \cdot e_{snow} \cdot s \cdot T_s(\vec{x})^4 + \\ & (1 - A_f) \cdot e_{ground} \cdot s \cdot T_a(\vec{x})^4\} \cdot (1 - V_d(\vec{x})) \end{aligned} \quad \text{(A24)}$$

The net longwave radiation at any location $\vec{x}$, is then computed as

$$R_{lw,net}(\vec{x}) = R_{lwi}(\vec{x}) - R_{lw,out}(\vec{x}) + R_{lwi,terrain}(\vec{x}) \quad \text{(A25)}$$

where $R_{lw,out}(\vec{x})$ is equal to $R_{lw,snow}(\vec{x})$ if the location has snow on the ground, or equal to $R_{lw,ground}(\vec{x})$ if the location is bare of snow.

The net radiation R_n (W m^{-2}) at any location $\vec{x}$, is then computed as

$$R_n(\vec{x}) = \left(1 - A(\vec{x})\right) \cdot \left(R_{dir}(\vec{x}) + R_{dif}(\vec{x})\right) + R_{lw,net}(\vec{x}) \quad \text{(A26)}$$

where A is the albedo of the surface determined based on surface properties (snow or vegetation/bare ground).

Acknowledgments

This work was supported by the Environmental Protection Agency (agreement no: R824784) under the National Science Foundation/Environmental Protection Agency Water and Watersheds program. The views and conclusions expressed are those of the authors and should not be interpreted as necessarily representing the official policies, either expresses or implied, of the US Government.

References

Cooley, K. R., (1988),"Snowpack Variability on Western Rangelands," in Western Snow Conference Proceedings, Kalispell, Montana, April 18-20.

Dingman, S. L., (1994), Physical Hydrology, Macmillan, 575 p.

Dozier, J. and J. Frew, (1990), "Rapid Calculation of Terrain Parameters for Radiation Modeling From Digital Elevation Data," IEEE Transactions on Geoscience and Remote Sensing, 28(5): 963-969.

Duffie, J. A. and W. A. Beckman, (1991), Solar Engineering of Thermal Processes, Second Edition, Wiley-Interscience, John Wiley and Sons, Inc., New York, 919 p.

Duffy, C. J., K. R. Cooley, N. Mock and D. Lee, (1991), "Self-affine scaling and subsurface response to snowmelt in steep terrain," Journal of Hydrology, 123: 395-414.

Erbs, D. G., S. A. Klein and J. A. Duffie, (1982), "Estimation of the Diffuse Radiation Fraction for Hourly, Daily and Monthly-Average Global Radiation," Solar Energy, 28: 293.

Flerchinger, G. N., K. R. Cooley, C. L. Hanson and M. S. Seyfried, (1998), "A uniform versus an aggregated water balance of a semi-arid watershed," Hydrological Processes, 12: 331-342.

Flerchinger, G. N., K. R. Cooley and D. R. Ralston, (1992), "Groundwater Response to Snowmelt in a Mountainous Watershed," Journal of Hydrology, 133: 293-311.

Hamon, W. R., (1973),"Computing actual precipitation," in Distribution of Precipitation in Mountainous Areas, Geilo Symposium, ed. WMO, Norway, World Meteorological Organization, Geneva, p.159-174.

Hanson, C. L., (1989), "Precipitation catch measured by the Wyoming shield and the dual-gage system," Water Resources Bulletin, 25: 159-164.

Jackson, T. H., D. G. Tarboton and K. R. Cooley, (1996), "A Spatially-Distributed Hydrologic Model for a Small Arid Mountain Watershed," Submitted to Journal of Hydrology, UWRL working paper WP-96-HWR-DGT/002.

Jackson, T. H. R., (1994), "A Spatially Distributed Snowmelt-Driven Hydrologic Model applied to the Upper Sheep Creek Watershed," Ph.D Thesis, Utah State University.

Kuczera, G., (1994), "NLFIT, A Bayesian Nonlinear Regression Program Suite," Version 1.00g, Department of Civil Engineering and Surveying, University of Newcastle, NSW, 2308, Australia.

Liston, G. E. and M. Sturm, (1998), "A Snow-Transport Model for Complex Terrain," Journal of Glaciology (in press).

Pomeroy, J. W. and D. M. Gray, (1995), Snowcover: Accumulation, Relocation and Management, National Hydrology Research Institute Science Report No. 7, Saskatoon, Saskatchewan, Canada, 144 p.

Riley, J. P., D. G. Chadwick and J. M. Bagley, (1966), "Application of electronic analog computer to solution of hydrologic and river basin planning problems: Utah simulation model II," PRWG32-1, Utah Water research lab., Utah State University.

Satterlund, D. R., (1979), "An Improved Equation for Estimating Long-wave Radiation From the Atmosphere," Water Resources Research, 15: 1643-1650.

Sharma, A. and D. G. Tarboton, (1995), "Conceptual Models of Snowmelt Processes," Eos Trans. AGU, 76(46): Fall Meeting Suppl., F203, Presentation at AGU fall meeting.

Shuttleworth, W. J., (1992), "Evaporation," Chapter 4 in Handbook of Hydrology, Edited by D. R. Maidment, McGraw-Hill, New York.

Stephenson, G. R. and R. A. Freeze, (1974), "Mathematical Simulation of Subsurface Flow Contributions to Snowmelt Runoff, Reynolds Creek Watershed, Idaho," Water Resources Research, 10(2): 284-294.

Stevens, G. R., (1991), "A geophysical investigation of the Upper Sheep drainage, Reynolds Creek Experimental Watershed, Owyhee County, Idaho," Master's Thesis, Geophysics Program, University of Idaho.

Tarboton, D. G., T. G. Chowdhury and T. H. Jackson, (1995a),"A Spatially Distributed Energy Balance Snowmelt Model," Biogeochemistry of Seasonally Snow-Covered Catchments, ed. K. A. Tonnessen et al., Proceedings of a Boulder Symposium, July 3-14, IAHS Publ. no. 228, p.141-155.

Tarboton, D. G., T. H. Jackson, J. Z. Liu, C. M. U. Neale, K. R. Cooley and J. J. McDonnell, (1995b),"A Grid Based Distributed Hydrologic Model: Testing Against Data from Reynolds Creek Experimental Watershed," in Preprint Volume, American Meteorological Society Conference on Hydrology, Dallas, Texas, January 15-20, p.79-84.

Tarboton, D. G. and C. H. Luce, (1996), "Utah Energy Balance Snow Accumulation and Melt Model (UEB)," Computer model technical description and users guide, Utah Water Research Laboratory and USDA Forest Service Intermountain Research Station (http://www.engineering.usu.edu/dtarb/).

U.S. Army Corps of Engineers, (1956), "Snow Hydrology, Summary report of the Snow Investigations," , U.S. Army Corps of Engineers, North Pacific Division, Portland, Oregon.

Wigmosta, M. S., L. W. Vail and D. P. Lettenmaier, (1994), "A Distributed Hydrology-Vegetation Model for Complex Terrain," Water Resources Research, 30(6): 1665-1679.

Winkelmaier, J. R., (1987), "Ground-water flow characteristics in fractured basalt in a zero-order basin," Master's Thesis, Hydrology Department, University of Idaho.

Table 1. Calibrated melt factors at USC (5 Par PDIMS).

Configuration	January	February	March	April	May
5 Par PDIMS	0.106	0.635	0.063	0.065	0.045

Table 2. Parameters of DZHM.

Parameter	Calibrated Value	Parameter	Prescribed Value
K_{veg} (Zone 1)	1.3960	θ_s (Zone 1)	0.54
K_{veg} (Zone 2)	1.4990	θ_s (Zone 2)	0.61
K_{veg} (Zone 3)	1.5999	θ_s (Zone 3)	0.70
K_0	0.2 m/hr	θ_r (Zone 1)	0.39
f	2.156 1/m	θ_r (Zone 2)	0.46
z_i	1.335 m	θ_r (Zone 3)	0.50
η	2.156	θ_w (Zone 1)	0.14
		θ_w (Zone 2)	0.21
		θ_w (Zone 3)	0.18
		z_r	0.75 m
		c	1.0

Table 3. Modeled Mass balance summary at USC (Oct. 1, 1992 to Aug. 16, 1993).

	Basinwide average	Zone 1 (48%)	Zone 2 (27%)	Zone 3 (25%)
Surface Water Input (mm)	715.2	460.0	665.3	1263.2
Potential Evapotranspiration (mm)	878.4	967.8	862.3	724.0
Actual Evapotranspiration (mm)	407.8	394.8	383.7	460.1
Change in Soil Storage (mm)	20.1	18.7	17.8	25.4
Change in Ground Water Storage (mm)	226.7	46.4	263.9	532.5
Modeled Runoff (mm)	60.6	0.0	0.0	245.2
Measured Runoff (mm)*	59.7	--	--	--

* measured basin average outflow

Captions for figures

Fig. 1. Reynolds Creek Experimental Watershed and Upper Sheep Creek, the first order subwatershed which is the focus of this study.

Fig. 2. The measured SWE maps during 1992-93 season. Measurements were made on a 30.48 m grid approximately aligned with the long axis of USC. These maps were produced by interpolation of measured data on to the 30 m north-aligned DEM grid.

Fig. 3. Drift factors at Upper Sheep Creek calibrated using UEB as the snowmelt model. The calibration used the first three measured SWE maps during 1992-93.

Fig. 4. Time series of basin average snow water equivalence at Upper Sheep Creek during 1992-93.

Fig. 5. Measured and modeled basin average snow loss rate between snow survey dates.

Fig. 6. SWE maps modeled by 5Par PDIMS during 1992-93 season.

Fig. 7. Comparison between 5Par PDIMS modeled and observed SWE at USC.

Fig. 8. Distribution of drift factors at Upper Sheep Creek. There are 275 grid cells in the watershed. Inset: Three zones of Upper Sheep Creek based on drift factor distribution. Zone 1:

$0.0 \leq DF < 0.5$ (47.64% of total area of USC), Zone 2: $0.5 \leq DF < 1.0$ (27.64%) and Zone 3: $1.0 \leq DF$ (24.72%).

Fig. 9. Time series of cumulative surface water input for the three zones at USC during 1992-93 as modeled by 5 Par PDIMS.

Fig. 10. Observed and modeled outflow hydrographs at Upper Sheep Creek during 1992-93.

Fig. 11. Moisture content based reduction function for actual evapotranspiration. θ_s is saturation moisture content, θ_r is the field capacity or drainable moisture content and θ_w permanent wilting point.

Fig. 12. Modeled and measured cumulative evapotranspiration.

Fig. 13. Cumulative basinwide mass balance plot for 1992-93. The difference between precipitation and surface water input is surface water storage as snowpack. The difference between the surface water input line and the evapotranspiration line is recharge which is available for runoff.

Fig. 1

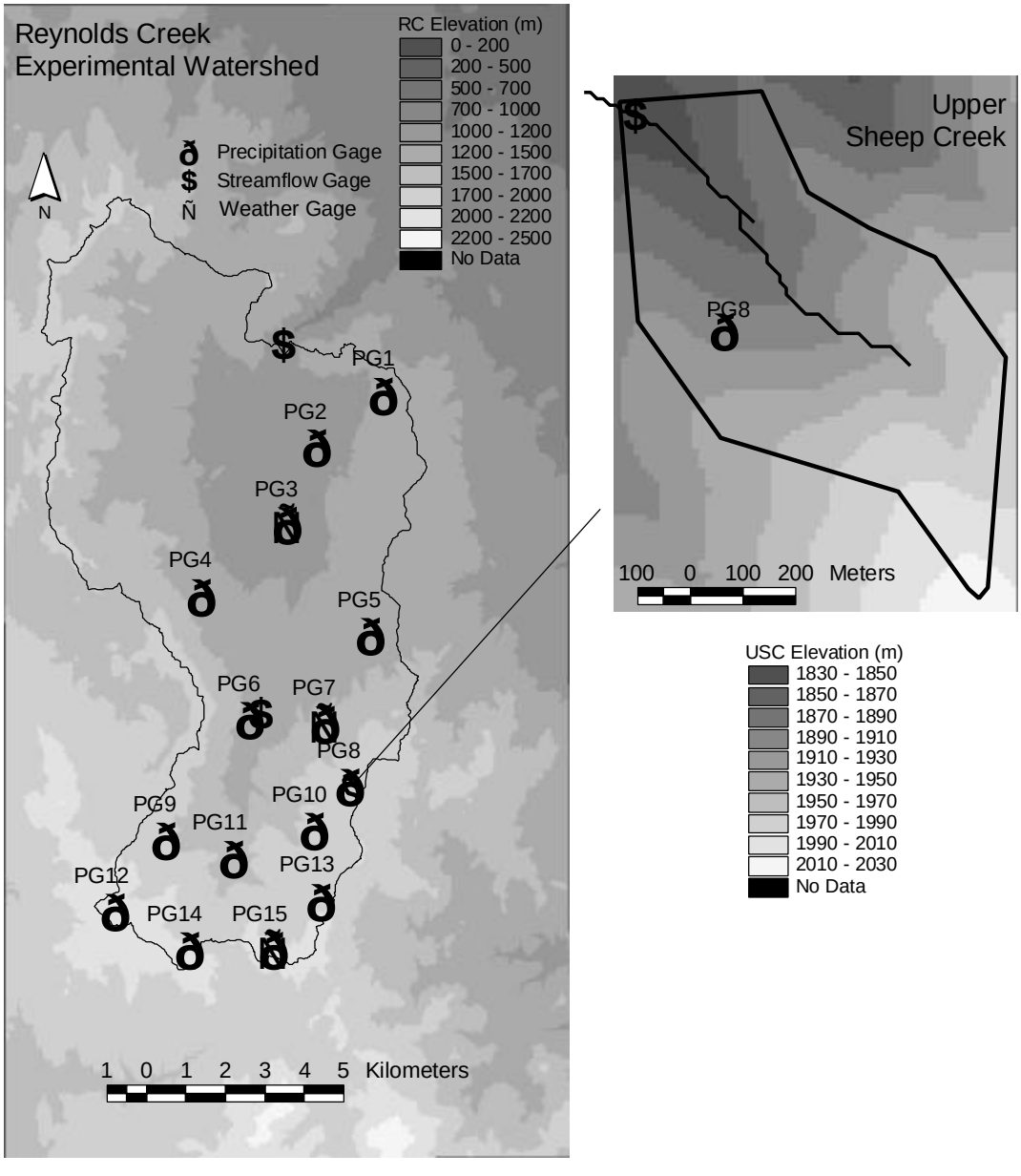
Reynolds Creek
Experimental Watershed
RC Elevation (m)
0 - 200
200 - 500
500 - 700
700 - 1000
1000 - 1200
1200 - 1500
1500 - 1700
1700 - 2000
2000 - 2200
2200 - 2500
No Data
Precipitation Gage
Streamflow Gage
Weather Gage
N
PG1
PG2
PG3
PG4
PG5
PG6
PG7
PG8
PG9
PG10
PG11
PG12
PG13
PG14
PG15
1 0 1 2 3 4 5 Kilometers
Upper
Sheep Creek
PG8
100 0 100 200 Meters
USC Elevation (m)
1830 - 1850
1850 - 1870
1870 - 1890
1890 - 1910
1910 - 1930
1930 - 1950
1950 - 1970
1970 - 1990
1990 - 2010
2010 - 2030
No Data

Fig. 2

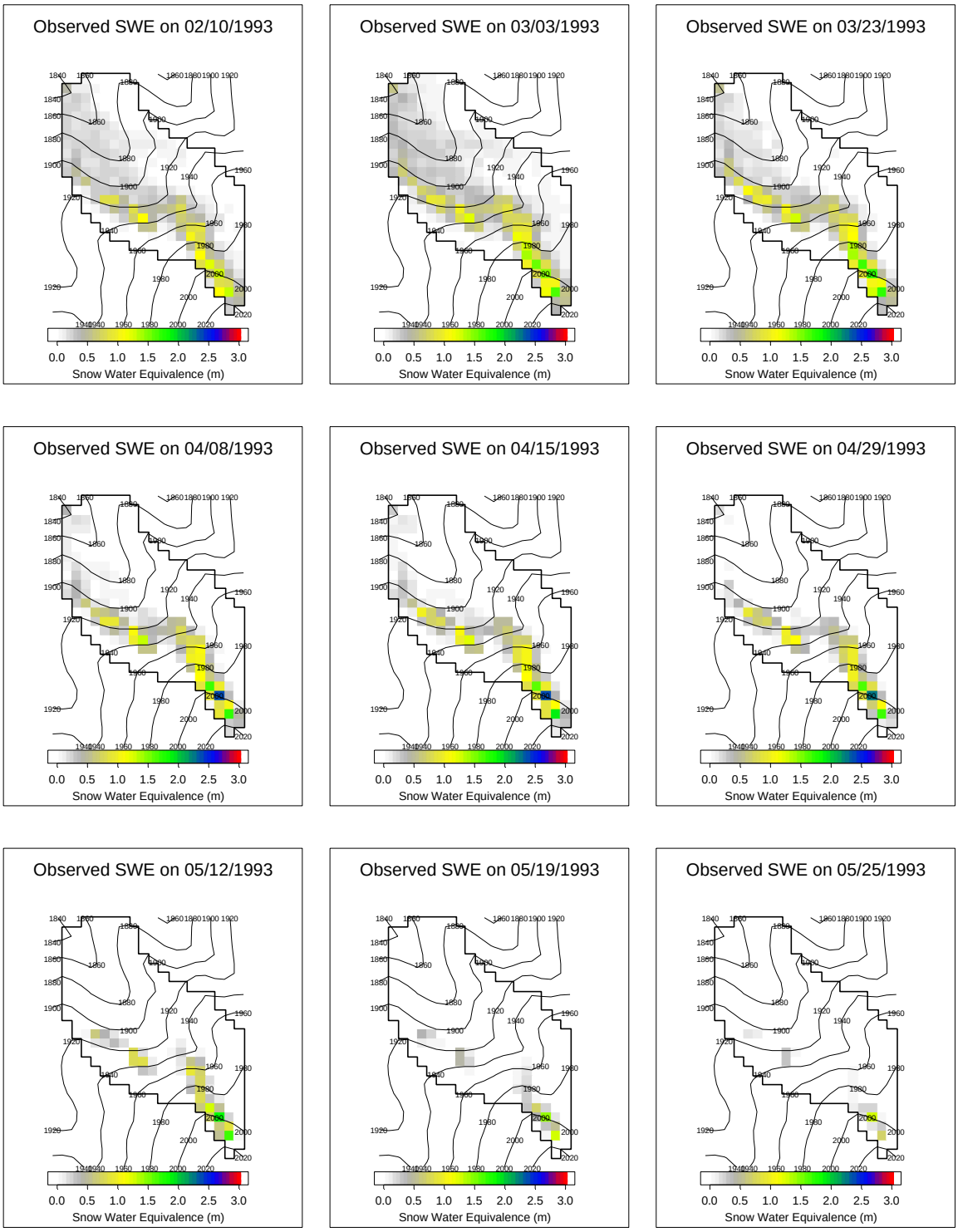
Observed SWE on 02/10/1993
Observed SWE on 03/03/1993
Observed SWE on 03/23/1993
Observed SWE on 04/08/1993
Observed SWE on 04/15/1993
Observed SWE on 04/29/1993
Observed SWE on 05/12/1993
Observed SWE on 05/19/1993
Observed SWE on 05/25/1993
0.0 0.5 1.0 1.5 2.0 2.5 3.0
Snow Water Equivalence (m)

Fig. 3

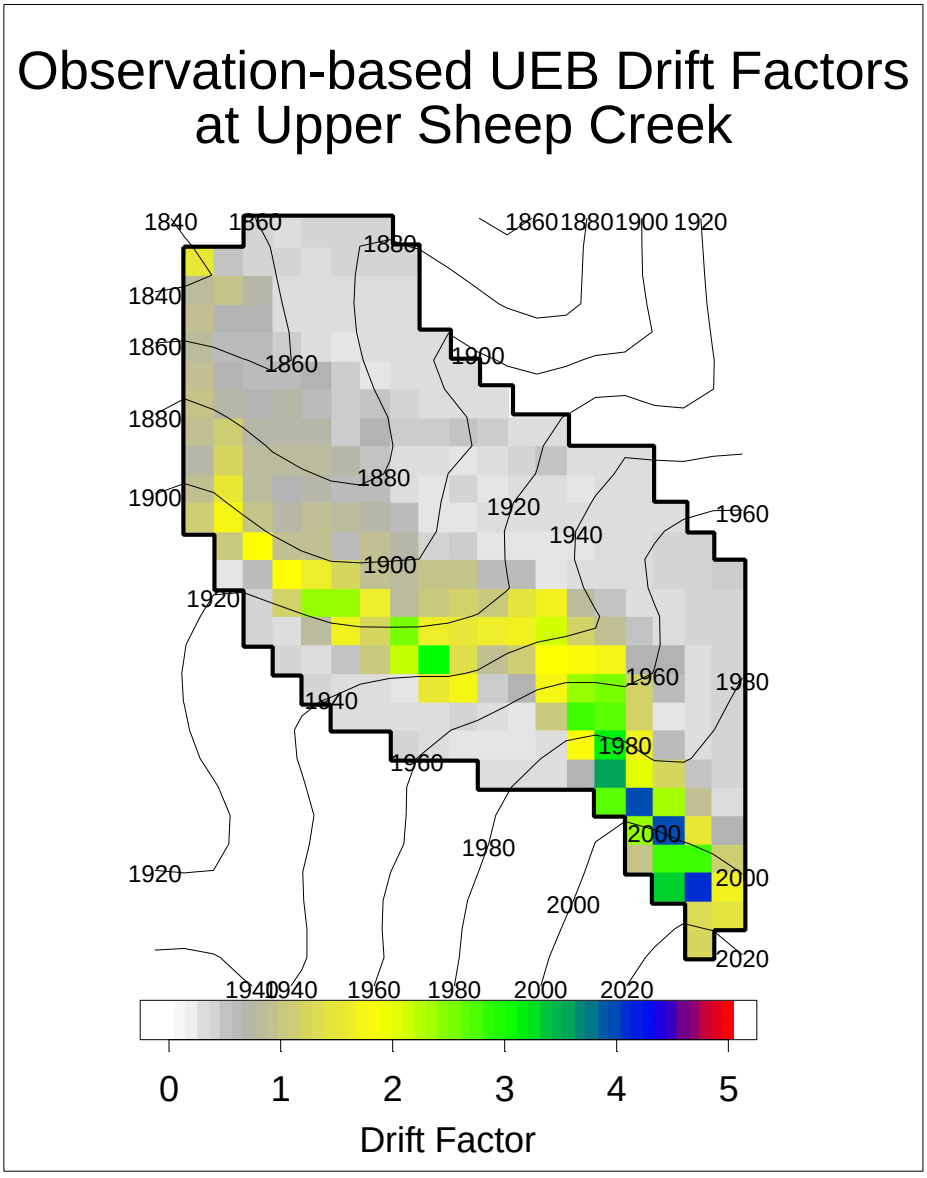
Observation-based UEB Drift Factors
at Upper Sheep Creek
1840
1860
1880
1900
1920
1940
1960
1980
2000
2020
0
1
2
3
4
5
Drift Factor

Fig. 4

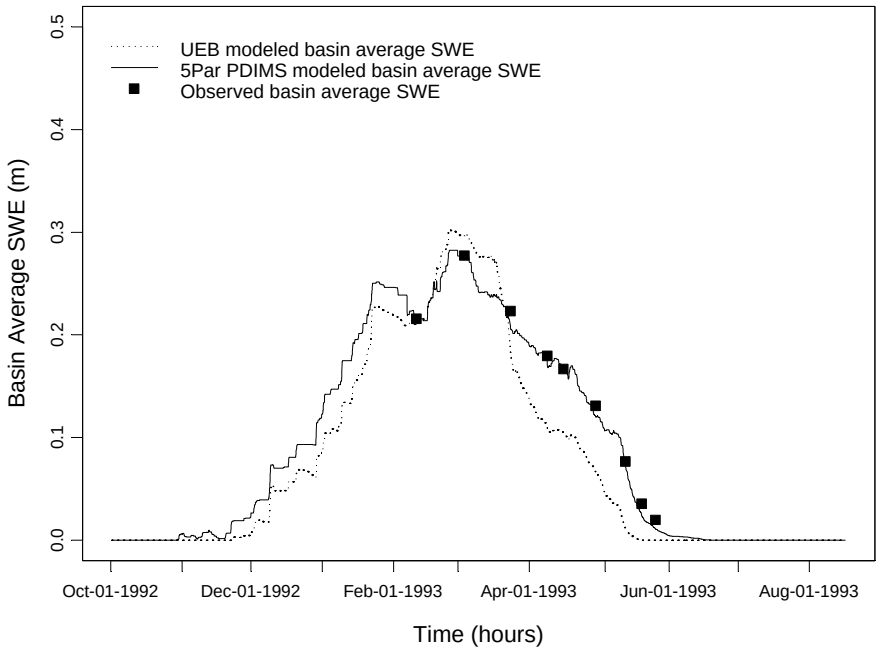
UEB modeled basin average SWE
5Par PDIMS modeled basin average SWE
Observed basin average SWE
Basin Average SWE (m)
0.0
0.1
0.2
0.3
0.4
0.5
Oct-01-1992
Dec-01-1992
Feb-01-1993
Apr-01-1993
Jun-01-1993
Aug-01-1993
Time (hours)

Fig. 5

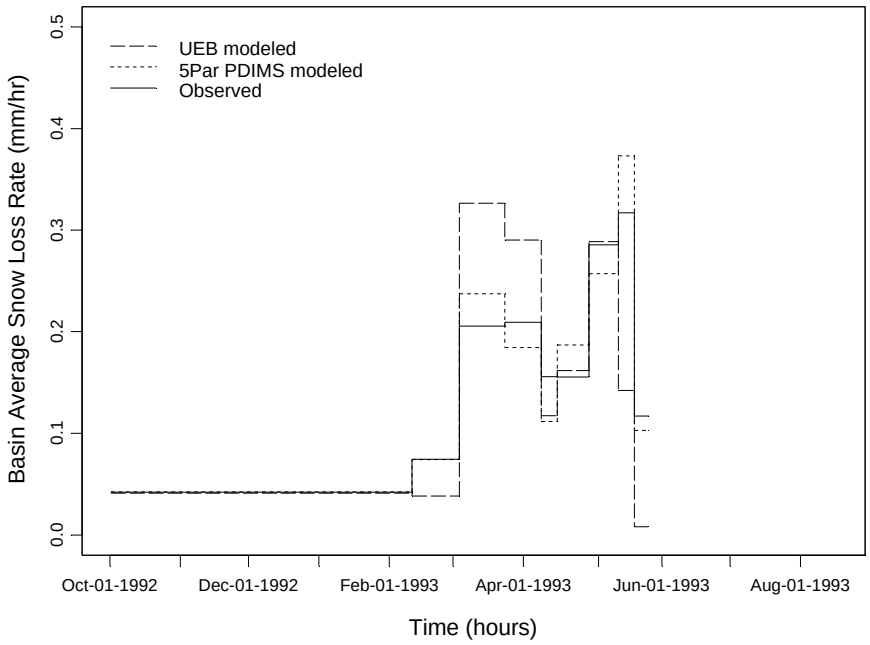
UEB modeled
5Par PDIMS modeled
Observed
Basin Average Snow Loss Rate (mm/hr)
0.0
0.1
0.2
0.3
0.4
0.5
Oct-01-1992
Dec-01-1992
Feb-01-1993
Apr-01-1993
Jun-01-1993
Aug-01-1993
Time (hours)

Fig. 6

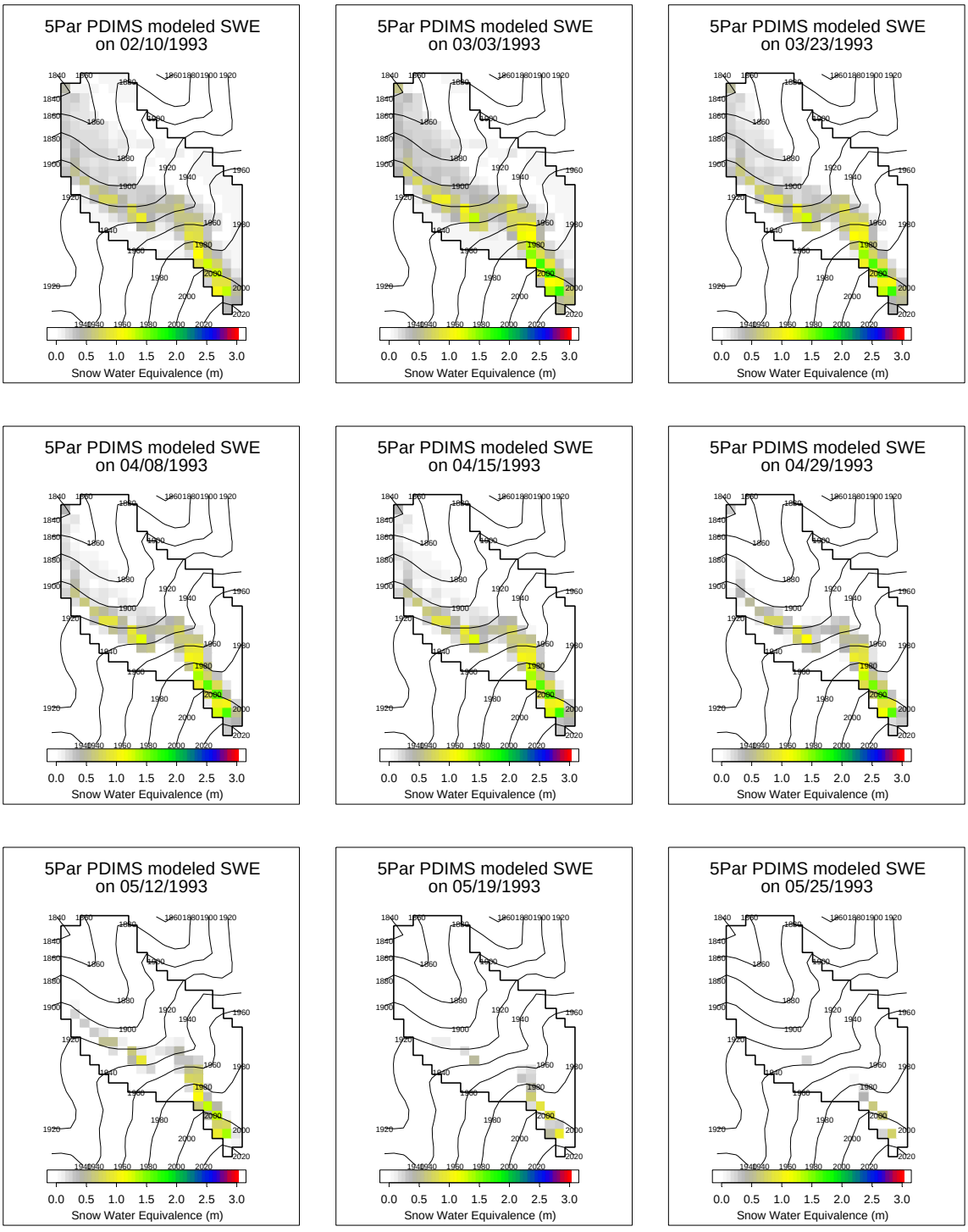
5Par PDIMS modeled SWE on 02/10/1993
5Par PDIMS modeled SWE on 03/03/1993
5Par PDIMS modeled SWE on 03/23/1993
5Par PDIMS modeled SWE on 04/08/1993
5Par PDIMS modeled SWE on 04/15/1993
5Par PDIMS modeled SWE on 04/29/1993
5Par PDIMS modeled SWE on 05/12/1993
5Par PDIMS modeled SWE on 05/19/1993
5Par PDIMS modeled SWE on 05/25/1993
0.0 0.5 1.0 1.5 2.0 2.5 3.0
Snow Water Equivalence (m)

Fig. 7

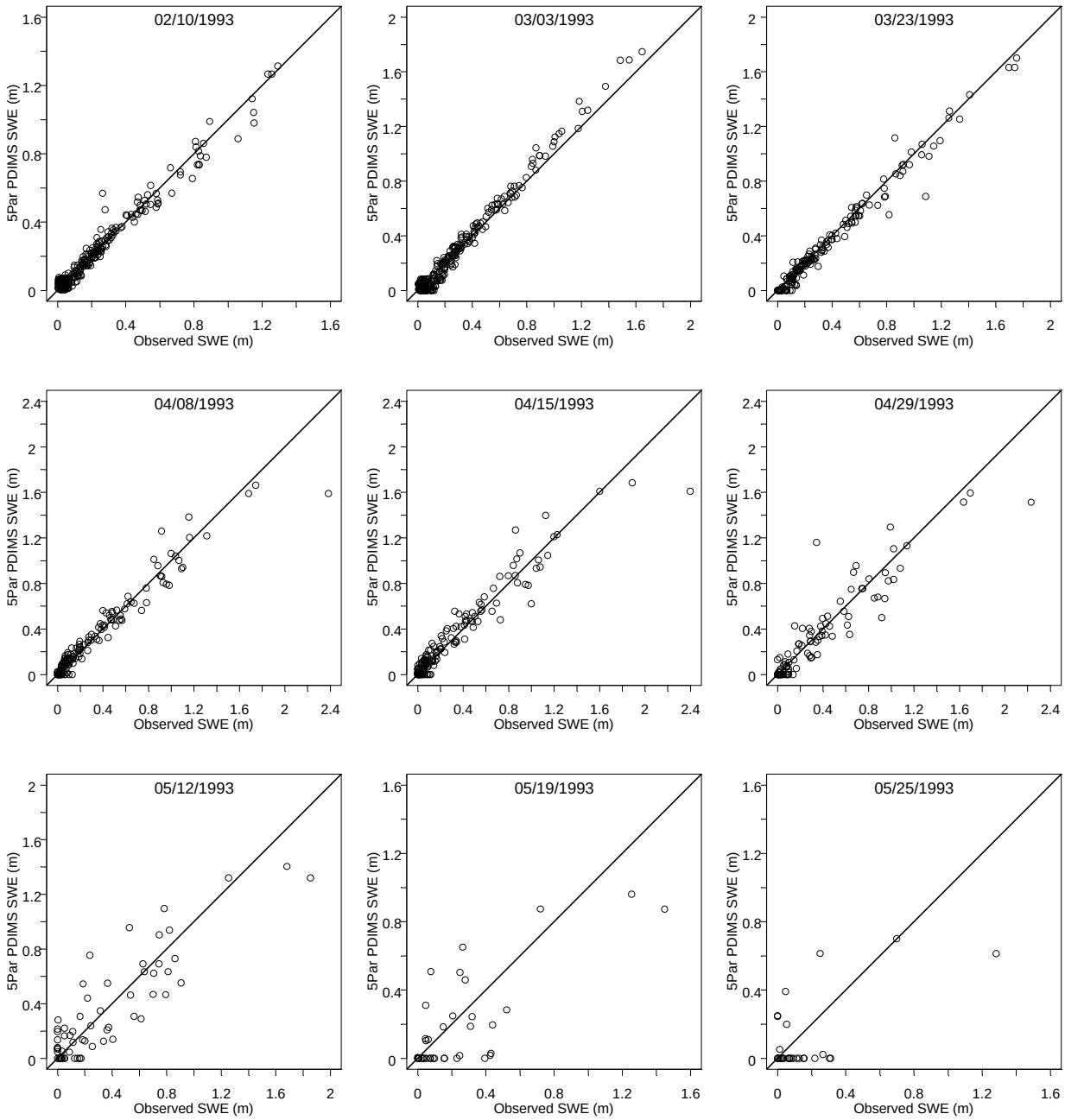
02/10/1993
03/03/1993
03/23/1993
04/08/1993
04/15/1993
04/29/1993
05/12/1993
05/19/1993
05/25/1993
5Par PDIMS SWE (m)
Observed SWE (m)

Fig. 8

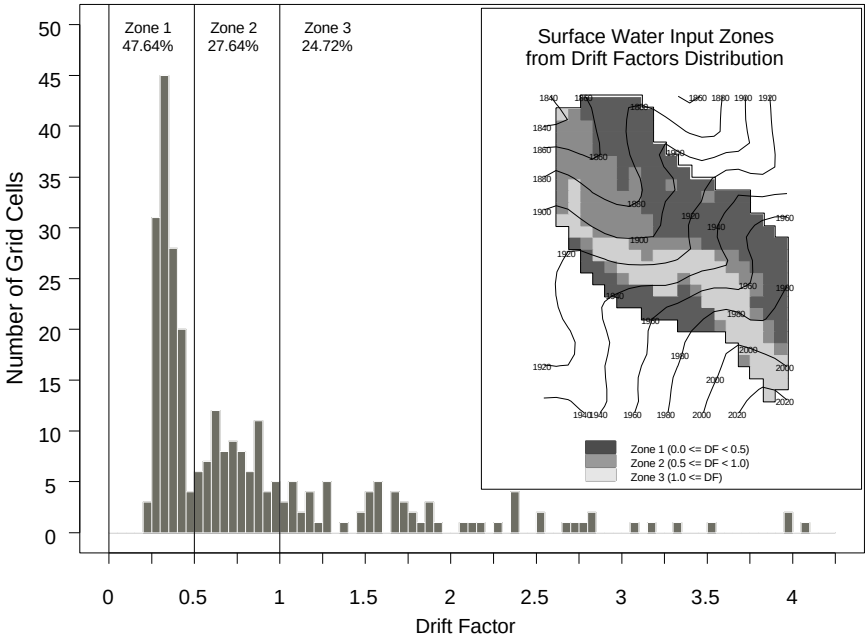
Zone 1
47.64%
Zone 2
27.64%
Zone 3
24.72%
Number of Grid Cells
Drift Factor
Surface Water Input Zones
from Drift Factors Distribution
Zone 1 (0.0 <= DF < 0.5)
Zone 2 (0.5 <= DF < 1.0)
Zone 3 (1.0 <= DF)

Fig. 9

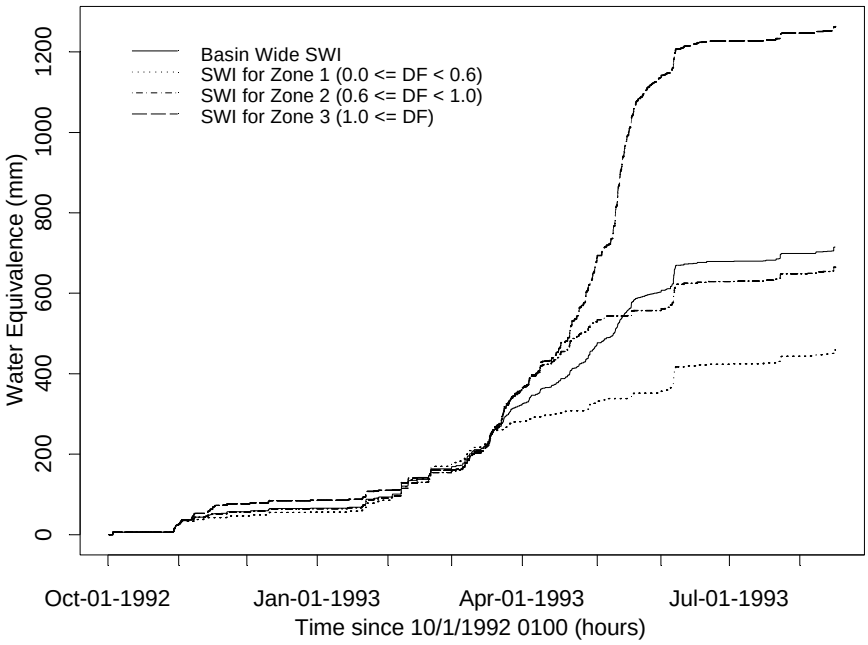
Basin Wide SWI
SWI for Zone 1 (0.0 <= DF < 0.6)
SWI for Zone 2 (0.6 <= DF < 1.0)
SWI for Zone 3 (1.0 <= DF)
Water Equivalence (mm)
0
200
400
600
800
1000
1200
Oct-01-1992
Jan-01-1993
Apr-01-1993
Jul-01-1993
Time since 10/1/1992 0100 (hours)

Fig. 10

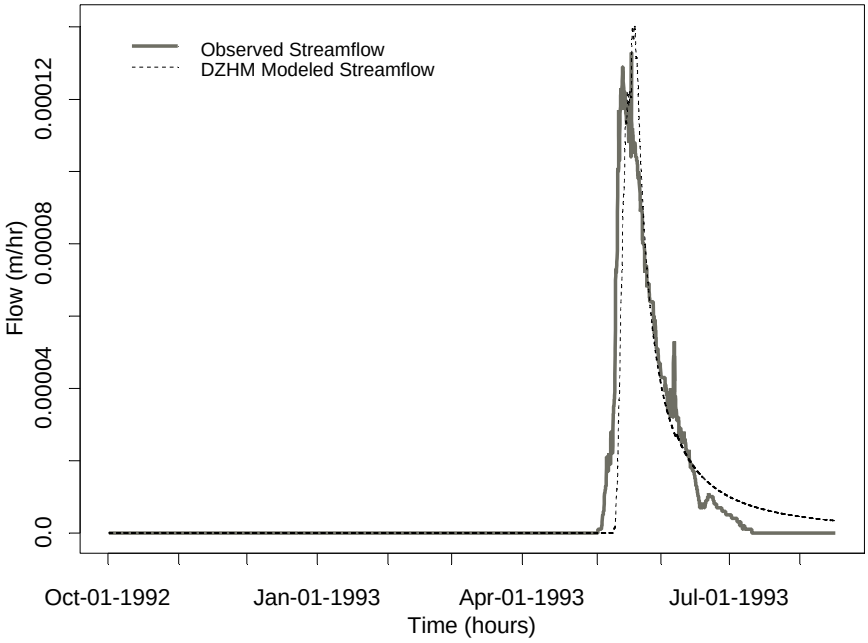
Observed Streamflow
DZHM Modeled Streamflow
Flow (m/hr)
0.0
0.00004
0.00008
0.00012
Oct-01-1992
Jan-01-1993
Apr-01-1993
Jul-01-1993
Time (hours)

Fig. 11

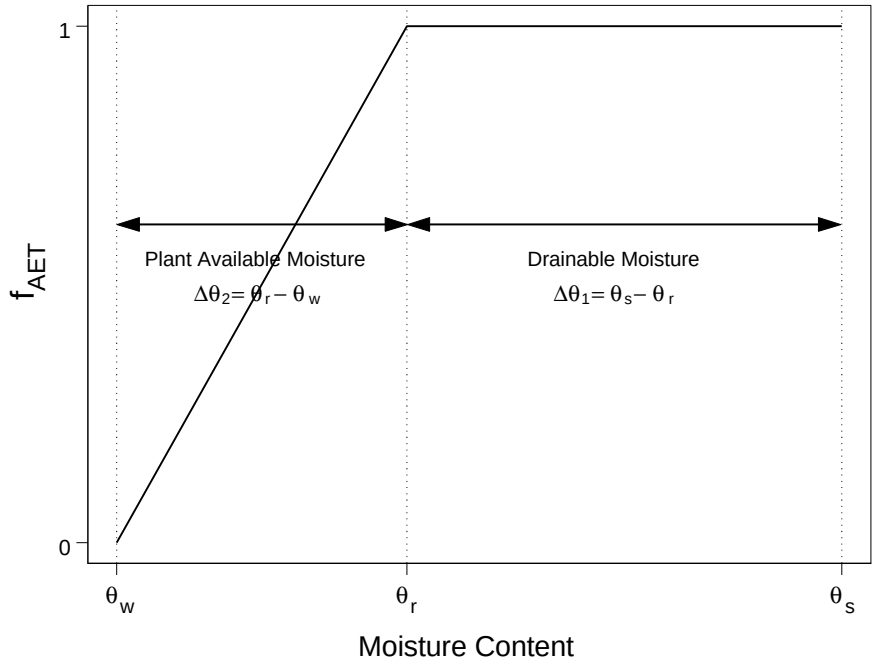
1
0
f_{AET}
Plant Available Moisture
$\Delta\theta_2 = \theta_r - \theta_w$
Drainable Moisture
$\Delta\theta_1 = \theta_s - \theta_r$
θ_w
θ_r
θ_s
Moisture Content

Fig 12.

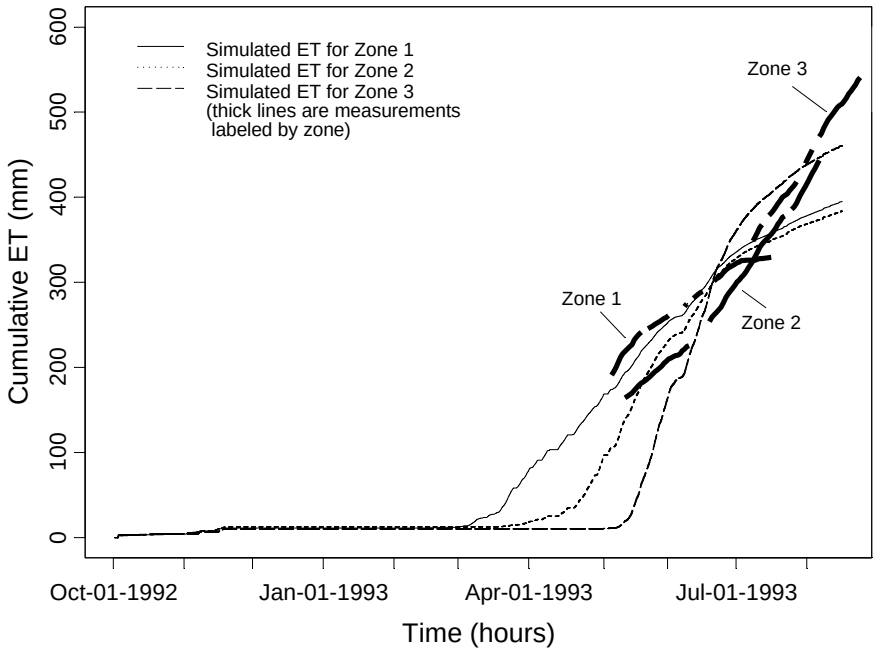
Simulated ET for Zone 1
Simulated ET for Zone 2
Simulated ET for Zone 3
(thick lines are measurements
labeled by zone)
Zone 1
Zone 2
Zone 3
Cumulative ET (mm)
0
100
200
300
400
500
600
Oct-01-1992
Jan-01-1993
Apr-01-1993
Jul-01-1993
Time (hours)

Fig. 13

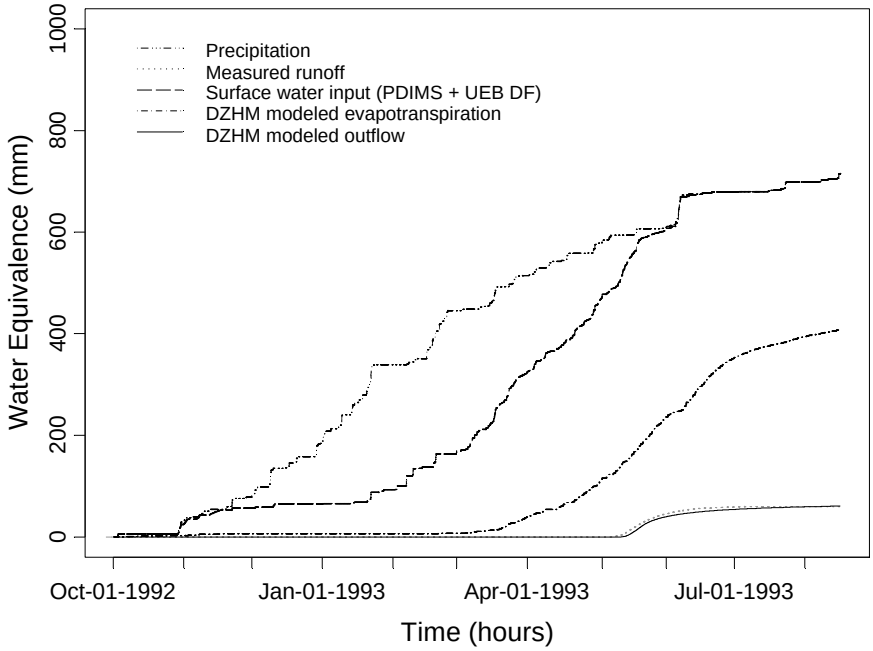
Precipitation
Measured runoff
Surface water input (PDIMS + UEB DF)
DZHM modeled evapotranspiration
DZHM modeled outflow
Water Equivalence (mm)
0
200
400
600
800
1000
Oct-01-1992
Jan-01-1993
Apr-01-1993
Jul-01-1993
Time (hours)